Macromolecules

Article

pubs.acs.org/Macromolecules

Distributions of a Linear Homopolymer Additive in an Ordered Block Copolymer Matrix As Quantified by Small-Angle Neutron Scattering

Hua-Gen Peng,[†,‡] Vikram K. Daga,[‡] Ying Lin,[‡] James J. Watkins,[*,§] Wen-Li Wu,[*,†] and Christopher L. Soles[*,†]

[†]Materials Science and Engineering Division, National Institute of Standards and Technology, Gaithersburg, Maryland 20899-1070, United States

[‡]Polymer Science and Engineering Department and [§]Department of Chemical Engineering, University of Massachusetts, Amherst, Massachusetts 01003, United States

Supporting Information

ABSTRACT: The addition of linear poly(acrylic acid) (PAA) to a disordered low molecular mass poly(ethylene oxide)−poly(propylene oxide)−poly(ethylene oxide) triblock copolymer host (PEO-*b*-PPO-*b*-PEO) is known to induce an ordering transition. Small-angle neutron scattering (SANS) measurements are presented to quantify the spatial distribution of the linear homopolymer additive within the ordered microstructure by using deuterium-labeled block copolymers. The analysis, however, requires revisiting the conventional algorithm of expressing the scattering intensity as a product of a form and structure factor, where the two terms are independent, and an alternate formalism is introduced that couples these terms. The SANS data are consistent with a lamellar morphology, but with the unusual caveat of a weak first-order scattering peak relative to a strong second-order peak. This necessitates the use of a four-layer structure for the lamellar repeat unit where the center of the PEO domain is enriched with PAA. The SANS data are fit to quantify the compositional profiles of the three components across the four-layer lamellar repeat unit. As the concentration and/or molecular mass of the PAA additive increases, PEO−PAA-rich and PPO-rich domains gradually emerge. However, it is not until relatively high PAA loadings that compositionally pure PPO domains appear. While the PAA additive is known to form hydrogen bonds with the PEO segments, the measurements suggest that the unfavorable interactions between the PAA and PPO are also important for driving the self-assembly process.

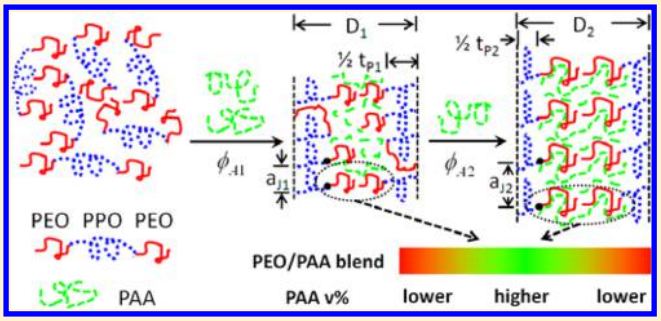

INTRODUCTION

Block copolymers (BCPs) are known to self-assemble into a range of morphologies with tunable dimensions at the nanoscale. Both the relative molecular masses of the different blocks (i.e., relative volume fractions) and the nature of the interactions between the blocks can be varied to achieve a breadth of different phase-separated morphologies. There are an increasing number of examples in the literature where this intrinsic propensity of BCP systems to self-assemble is leveraged to template or to direct the self-assembly of other additives such as inorganic precursors,[1−3] hydrogen bonding small molecule organics,[4−6] salts or ions,[7−11] nanoparticles,[12−28] and homopolymers.[6,29−41] All of these examples leverage the thermodynamic parameters of mixing to selectively drive or sequester the additive into one of the BCP domains. A common design cue is to tailor the enthalpic interactions between the additive and one of the blocks to be favorable and thereby selectively drive the additive into that domain. There are numerous examples of where enthalpy is used to control the dispersion of inorganic and small molecule precursors,[2−6] nanoparticles,[12−17] and homopolymer[6,37−41] additives in block copolymer matrices. In addition to enthalpy, one can also leverage the entropy of mixing to further tailor the dispersion of either functionalized nanoparticles[18−28] or linear homopolymers[29−36] within a BCP morphology. To fully understand these self-assembly and dispersion processes, one must consider both the enthalpic and entropic contributions to the free energy of mixing and self-assembly.

While these simple but eloquent concepts have been discussed and deployed on numerous BCP−additive systems, there is in general limited quantitative information on the spatial distribution and local composition of the additive within the different BCP phases. The best examples of spatially pinpointing the additive location within one of the BCP domains come from inorganic nanoparticles functionalized with organic ligands. Kramer and co-workers have shown that by tuning the enthalpic interactions of the ligand with the different blocks, one can control whether the nanoparticles reside selectively in the center of one of the domains or at the interface between the two blocks.[13−16] Others have shown that

Received: May 29, 2015
Revised: September 3, 2015
Published: October 7, 2015

DOI: 10.1021/acs.macromol.5b01163
Macromolecules 2015, 48, 7574−7584

by changing the size of the nanoparticle, one can tune the entropy of mixing and also control whether the nanoparticle resides at the center of one of the domains or the interface between them.[18−21,23,24] In fact, entropy can be a powerful tool for the controlling the organization of the nanoparticle additives within the BCP domains. Xu and co-workers have shown using rod−coil BCPs that entropy and enthalpy can be used together to assemble the nanoparticles into highly ordered arrays within one of the domains.[25−28] In almost all of these examples, the spatial distribution of the nanoparticles in the BCP matrix is quantified by either electron microscopy or computer simulation and modeling. The high z contrast between the nanoparticle and the matrix and the real space images provided by these techniques make characterizing the spatial distribution of the nanoparticle additives straightforward.

There is considerably less literature on trying to spatially resolve where a linear homopolymer additive resides within a BCP matrix. This is in part due to the experimental difficulty in trying to distinguish the linear additive from the BCP matrix. There have been several studies focused on systems where the homopolymer additive is identical to one of the blocks. In this regime the enthalpic interactions are negligible and entropy largely controls the distribution of the linear additive. These measurements show that low molecular mass homopolymers tend to be uniformly solubilized across their native domain while their high molecular mass analogues tend to segregate in the center of the native domain. Most of this knowledge has been derived indirectly from small-angle X-ray scattering (SAXS) measurements that quantify the long period and the thicknesses/dimensions of the different phases in the repeat unit. By knowing how the linear additive swells the selective phase relative to the excluded phase, one can infer if the distribution is uniform and isotropic, which increases the interfacial area between the phases, or localized to the center of the selective domain.[30−33,36] There have been a few examples validating these homopolymer distributions through either small-angle neutron scattering (SANS) measurements using deuterium-labeled polymers that increase contrast between the linear additive and the BCP matrix[34,35,42] or quantitative mean field calculations.[29] However, in general there is much less quantitative information about the distribution of linear homopolymer additive across the BCP domains. This is especially true in the limit where the homopolymer exhibits specific interactions with one of the BCP segments. This is the case of study in the current article.

The work presented here is an extension of previous studies where strongly interacting additives are used to induce the self-assembly of low molecular mass BCPs that otherwise exist as a disordered melt. The phase separation of BCPs into nanoscale domains is driven by the product χN, where χ is the Flory−Huggins interaction parameter between the dissimilar blocks and N is their degree of polymerization. Phase separation is promoted by both a high molecular mass and repulsive interactions between the blocks. There is considerable interest in reducing the size of the self-assembled domains by using shorter block lengths. However, small BCPs can lack the driving force to phase segregate due to their small N and therefore remain disordered. This imposes practical limits on how small the phase-separated domains can be. An effective alternative is to incorporate additives that have selective interactions with one of the blocks. Previously, we have shown how this can create very fine ordered nanostructures using low molecular mass Pluronic surfactants, poly(ethylene oxide)−poly(propylene oxide)−poly(ethylene oxide) triblock copolymers (PEO-*b*-PPO-*b*-PEO), that are commercially available. This has been demonstrated with all of the different types of additives discussed thus far, including small molecular and inorganic precursors,[3,5,43] nanoparticles,[12] and strongly associating linear homopolymers.[6,37] We have even shown that photoactive small molecules that switch their hydrophobic/philic nature up exposure to UV radiation can be used to realize photoinduced ordering of the Pluronics template.[4]

The focus of the current article is to elucidate the physics of this additive driven self-assembly mechanism when the linear homopolymer additive, poly(acrylic acid) (PAA), has a strong affinity for PEO block of the Pluronic surfactant. We take advantage of a deuterium labeling scheme to control the contrast between the linear additive and the BCP matrix and introduce a new quantitative SANS formalism to spatially resolve the compositional profiles of the linear additive across the domains of a phase-separated morphology. This analysis reveals the physical mechanism by which the linear PAA additive gradually extracts the PPO segments out the disordered PEO-*b*-PPO-*b*-PEO melt and into well-ordered lamellar structure. As linear PAA is progressively added to the system, the domains of the phase-separated PPO become increasingly rich until eventually a pure PPO domain is obtained. We believe that both the insight into this self-assembly mechanism and the generality of the SANS analysis method will have applicability to other kinds of strongly interacting additives such as small molecules, polymers, and nanoparticles.

■ RESULTS AND DISCUSSION

It is generally accepted that the linear PAA homopolymer prefers to associate with the PEO segments of the PEO-*b*-PPO-*b*-PEO BCP. Hydrogen-bonded complexes form between the PAA and PEO, as evidenced by the fact that PAA will solvate linear PEO and suppress its crystallization. However, the repulsive interactions between PEO and PPO are still relatively weak; PEO and PPO can coexist in a low molecular mass phase mixed melt. This is why the neat BCP copolymer studied here exists as a disordered melt. But the fact that PEO and PPO are not too different also implies that the repulsion between PPO and PAA is not that strong. In other words, the preference for PAA to associate with the PEO over PPO is not that strong. The central issue then becomes: what drives the PAA homopolymers interactions with the disordered melt, and how does the resulting phase-separated structure evolve?

We have already discussed how SANS measurements are sensitive to structures that have a strong difference in their scattering length densities (SLDs). If all three components are hydrogenated, the PAA has the largest SLD due to its low H content and highest mass density. The SLD of PAA is more than twice of that of PEO and about 5 times of that of PPO. This means that the SANS SLD contrast will be strongest between the hydrophilic (PAA + PEO) and hydrophobic (PPO) domains which makes it is difficult to discern the distribution of PAA inside the PEO; the natural SLD contrasts make this a difficult measurement. Therefore, we synthesized deuterium-labeled BCPs. The PEO blocks are fully deuterated (d-PEO), giving them the highest SLD of the three components in this system. The PPO is partially deuterated (65% d-PPO), having an intermediate SLD, by copolymerizing deuterated and hydrogenated propylene oxide monomers. The PAA homopolymer that is blended with the BCPs is fully

DOI: 10.1021/acs.macromol.5b01163
Macromolecules 2015, 48, 7574−7584

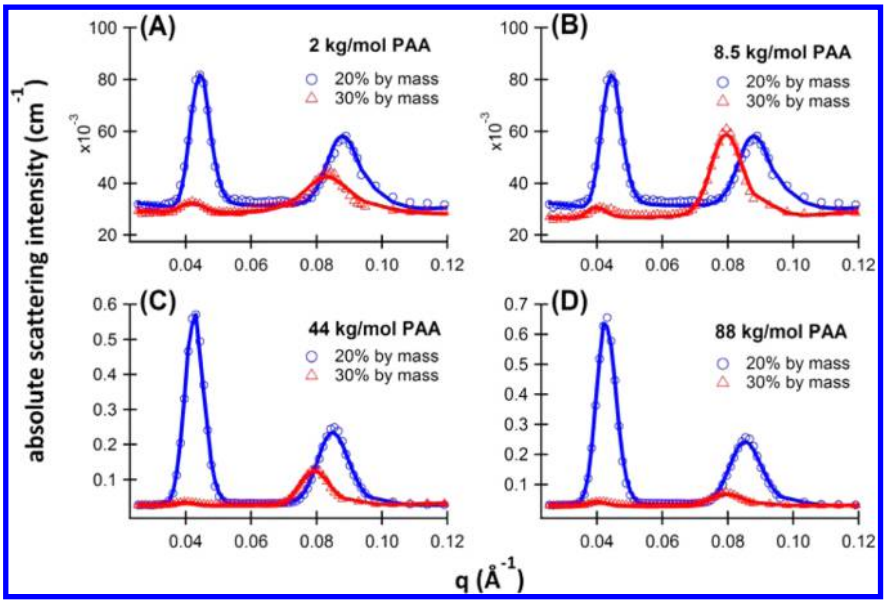

Figure 1. SANS results presented as scattering intensity versus q for the different PAA homopolymer, PEO−PPO−PEO BCP blends studied here. Parts A, B, C, and D correspond to PAA homopolymer additives with molecular masses of 2, 8.5, 44, and 88 kg/mol, respectively. Within each panel the open circles (blue) correspond to a PAA loading of 20% by mass while the open triangles (red) correspond to a loading of 30% by mass. The scattering intensities are presented on an absolute scale with no vertical shifts in the data. The solid lines represented the best fits using the formalism described later in the article. The standard uncertainties in the scattering intensities are all less than the size of the data markers.

hydrogenated (h-PAA), now having the lowest neutron SLD of the three components. With these isotopically labeled BCPs, we prepared two sets of blends. In "PAA-20", the PAA loading in the BCP is 20% by mass; in "PAA-30", the PAA loading is 30% by mass. These levels of deuterium substitution and mass loadings were designed to minimize the scattering contrast from the ordered BCP structure and focus on the conformation of PAA molecules; for the PAA-30 sample the SLD of the d-PEO and h-PAA mixture is 4.57×10^{-6} Å^{-2}, which comes close to contrast matching the partially deuterated PPO domains. A similar strategy was implemented by Quan et al. when trying to characterize the single chain confirmation of a high molecular mass poly(butadiene) homopolymer dispersed in a poly(styrene−butadiene−styrene) triblock copolymer host.[44]

Our assumption for choosing these levels of deuterium substitution, that the PAA distributes uniformly across the PEO domains, turned out to be incorrect. However, the subdued contrast between the hydrophilic and hydrophobic domains of the BCP structure enables us to quantify the compositional gradients of the PAA in the PEO domains. We utilized four different PAAs with mass averaged molecular masses of 2, 8.5, 44, and 88 kg/mol to explore how the molecular mass of the linear additive and its loading affect the blend morphology. The different blends are identified as 2k-20, 2k-30, 8k-20, 8k-30, 44k-20, 44k-30, 88k-20, and 88k-30, respectively, where "20" and "30" behind the dash denote the mass % loading of PAA in the BCP matrix.

SANS Results. Recently we reported SAXS measurements for these same systems[6,37] (albeit not the deuterium-labeled versions), and the SANS data presented here are fully consistent with our previous results. At 70 °C the neat BCP is disordered while the SAXS data on both PAA-20 and PAA-30 indicate a lamella structure as evident from the equally spaced first-, second-, and third-order diffraction peaks (see Figure S1 in the Supporting Information). The SANS data presented in Figure 1 also support a lamellar structure, but not the type with uniform SLD within individual lamellar domain as evidenced by the following key observation. Note that in the 20% blends the first-order scattering peaks are the most intense, but in the 30% blends the second-order peak is significantly more intense than the first-order one. The low first-order peak intensity in PAA-30 blends indicates that the SLD fluctuations averaged across a lamellar repeat are small, consistent with the fact that the SLD of the PEO and PAA mixture is close to that of the PPO at 30% by mass loading of the PAA. The intense second-order peaks indicate that strong SLD fluctuations exist at a length scale *smaller* than the lamellar repeat length. We explore this observation in greater depth below after a brief discussion of the basic scattering theory.

For lamellar structures the scattering intensity $I(q)$ is traditionally modeled as the product of two one-dimensional factors in Fourier space; the amplitude of the form factor, $F(q)$, which describes the shape of the scattering entity, and the structural factor, $S(q)$, which describes the lattice on which this scattering entities are repeated. In these factors q denotes the amplitude of the scattering vector as $(4\pi/\lambda)\sin(\theta/2)$, where θ is the scattering angle. In the past, $S(q)$ has been modeled in terms of the paracrystallinty model that allows for fluctuations of the lattice spacing.[32] For this moment we accept this conventional approach of treating $I(q)$ as a product of $F(q)$ and $S(q)$ as an approximation in order to guide our discussion below. The relation of $I(q) = S(q)F(q)$ will be re-evaluated later. The existence of a weak first-order peak and a strong second-order peak likely originates in $F(q)$ for the repeating unit since $S(q)$ for a simple lattice structure will always result in a continual decrease in intensity with q. A conventional form factor for a scattering entity with a simple two-phase SLD will also always result in first-order peak that is stronger than the any of the higher-order peaks. The observation of a weak first-order peak in comparison to the second-order peak necessitates the introduction of a structural entity with an intricate SLD. An example of this type of effect is seen in the scattering from particles precipitated out of a solid solution of AlAg.[46] The precipitation of Ag into nanoscale particles creates adjacent

DOI: 10.1021/acs.macromol.5b01163
Macromolecules 2015, 48, 7574−7584

rings around the particles that are depleted in Ag compared to the overall composition of the solid solution. In this system the average SLD over any distance greater than the particle diameter is equal to that of the surrounding. This leads small-angle X-ray scattering intensities to start low in the low q region and increases with q to a distinct maximum followed by the conventional decrease with q. This behavior is not observed when the scattering entity or the repeating unit is a distinct two-phase system where the value of $F(q = 0)$ is always at its maximum.

In this work we adopt a multilayer SLD profile that is analogous to the composition profiles in of AlAg particles as the building blocks for the lamellar structure. The essence of the proposed building block is to allow for a possible enrichment of PEO near the interfaces between the PAA and the PPO domains as shown in Figure 2. Chain connectivity mandates

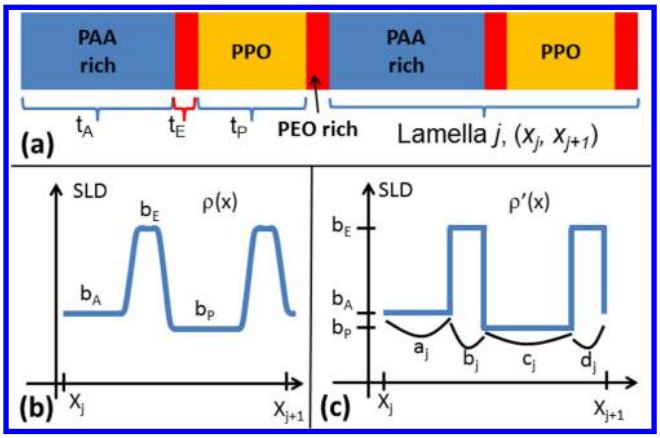

Figure 2. (a) Schematic depiction of the four-layer lamellar model for the PAA-Pluronic acid blends. (b) SLD profile with smooth interface between adjacent layers. (c) Same SLD profile as in (b) but with sharp interfaces between adjacent layers.

that PEO be adjacent to the PPO but the PAA has the freedom to distribute itself nonuniformly within the PEO-rich domains; the proposed repeating unit in Figure 2 is a logical first approximation for the lamellar form factors. The resulting form factor essentially becomes a four-layer model as pictorially shown in Figure 2a while the neutron SLD profiles in Figure 2b,c emphasize where the scattering contrast originates. The profile in Figure 2b is simply a derivation of the sharp interface model of Figure 2c, created by invoking a composition gradient at all of the interfaces. For simplicity, the sharp interface profile in Figure 2c will be used to calculate the volume fractions of PAA, PEO, and PPO in each of the layers while the symmetrically graded interface SLD profile in Figure 2b will be used to fit the actual SANS data. This four-layer SLD building block is analogous to the $F(q)$ form factor used to fit the scattering intensities from the previously mentioned AlAg particles and known to give rise to reduced intensities in the lower q region of the scattering.

Modeling of SANS Results. Now we revisit the validity of the relation $I(q) = F(q)\ S(q)$. To model the scattering intensities from an ordered block copolymer structure, one typically uses an expression similar to that derived by Guinier:[47]

$$I(\mathbf{q}) = N[\overline{f_n^2} - (\overline{f_n})^2] + (\overline{f_n})^2[N + \sum\sum \overline{\cos(2\pi\mathbf{q}\cdot\mathbf{x}_{nn'})}] \quad (1)$$

In this expression the term with double summation represents the structure factor $S(q)$, describing the relative positions of the N particles or scattering entities. The form factor for each of the scattering particles is $f_n(q)$, and by convention the q is dropped in eq 1. The term $(\overline{f_n})^2$ in the above equation is identical to form factor $F(q)$ discussed in the previous section. Such a separation or decoupling between the form factor and the structural factor has become common practice in analyzing the scattering from block copolymer structures. However, it is noteworthy that the above expression is actually a simplification from a more general equation which precedes eq 1 in ref 47:

$$I(\mathbf{q}) = N[\overline{f_n^2} + \sum\sum \overline{f_n f_{n'} \cos(2\pi\mathbf{q}\cdot\mathbf{x}_{nn'})}] \quad (2)$$

In metals or other atomic substance f_n is the form factor of each atom n and independent of the atomic position $\mathbf{x}_{nn'}$ or the corresponding structure factor. In this situation the decoupling of the form and structure factors is valid. However, for many incompressible structures, including BCP lamellar stacks, the above decoupling is strictly not valid. The thickness of lamellar block n, which dictates the form factor f_n, is also the distance between blocks n and $n + 1$ which locally determines the structure factor. It is simply incorrect to use an expression invoking the separation of the form factor and structure factor:

$$\sum\sum \overline{f_n f_{n'} \cos(2\pi\mathbf{q}\cdot\mathbf{x}_{nn'})} \neq \sum\sum \overline{f_n f_{n'}}\ \overline{\cos(2\pi\mathbf{q}\cdot\mathbf{x}_{nn'})} = (\overline{f_n})^2 S(\mathbf{q}) \quad (3)$$

This inequality remains true for many other block copolymer structures as well as systems like densely packed spheres where the only interparticle potential is the hard-core interaction among particles; the form and structure factors are coupled. In the ideal limit of a scattering system with uniformly sized particles or lamella with a monodispersed thickness, using the expression where the amplitude of the form and structure factors are decoupled will still yield correct results. However, as soon as fluctuations in lamellae thickness, particle size, or lattice parameters are allowed, the decoupling becomes invalid. In block copolymers these conditions are readily achieved through effects like thermal fluctuations or polydispersity in molecular mass, invalidating the assumption of decoupling. To the best of our knowledge, we are unaware of a proper treatment of these effects when interpreting the X-ray or neutron scattering from block copolymer systems.

In the following section an expression for the scattering intensity is derived based on lamellar structure where each repeat is composed of four layers as depicted in Figure 2. We start with a simplified model where the interface between different layers is sharp and the SLD for two PEO-rich layers are identical. The SLDs of the PEO-rich, PAA-rich, and PPO layers are denoted as b_E, b_A, and b_P, respectively. Within each repeating stack j, there are the four layers consecutively arranged as PAA-rich, PEO-rich, PPO, and PEO-rich layers with corresponding thickness of a_j, b_j, c_j, and d_j, respectively. Through eq 4, x_j and x_{j+1} define the position of the jth and $(j + 1)$th stacks in the repeating structure:

$$x_{j+1} = x_j + a_j + b_j + c_j + d_j \quad (4)$$

Using these definitions, the structure factor for the SLD profile of the lamellar structure with sharp interfaces (Figure 2c) can be expressed as

DOI: 10.1021/acs.macromol.5b01163
Macromolecules 2015, 48, 7574−7584

$$\rho'(x) = b_E + \sum_{j=1}^{N} PAA_j(x) + \sum_{j=1}^{N} PPO_j(x) \quad (5)$$

$$PAA_j(x) = \begin{cases} b_A - b_E & \text{for } x_j \le x \le x_j + a_j \\ 0 & \text{else} \end{cases} \quad (6)$$

$$PPO_j(x) = \begin{cases} b_P - b_E & \text{for } x_j + a_j + b_j \le x \le x_j + a_j + b_j + c_j \\ 0 & \text{else} \end{cases} \quad (7)$$

In these expressions the SLDs are all referenced relative to that of the PEO-rich layer (b_E) because it is the square of the difference of the SLDs that determines the scattering intensities. This is equivalent to assigning the PEO-rich layers SLD to zero in the repeat unit of Figure 2a; this is advantageous because two out of four layers correspond to these PEO-rich domains. This selection of b_E as the baseline helps simplify the full set of scattering equations that are provided in the Supporting Information.

We further assume that within each layer the thickness fluctuates with a Gaussian distribution independently around an average value. Mathematically, the distribution in thickness, a, of the PAA layers can be described by a simple Gaussian function:

$$p(a) = \frac{1}{\sqrt{2\pi}\, d_A} \exp\left[-\frac{(a - t_A)^2}{2{d_A}^2}\right] \quad (8)$$

where t_A is the average value and d_A denotes the standard deviation. This results in the smooth interfacial SLD profiles shown in Figure 2b.

The scattering intensity can be expressed as the product of the Fourier transform (FT) of the SLD profile and the corresponding conjugate of the FT:

$$I_1(q) = \mathrm{FT}\{\rho'(x)\}\cdot \mathrm{FT}^*\{\rho'(x)\} \quad (9)$$

which properly accounts for all of the scattering cross-terms when the form and structure factor are coupled. An explicit expression for this equation is provided in the Supporting Information and not be repeated here due to its length. Only the Fourier transforms of the layer thickness distribution functions are present in the expression for $I_1(q)$; there is no need for a structure factor $S(q)$ with additional independent parameters. This is expected since all the x_j, x_{j+1}, etc., terms are expressed as a summation of lamellar thickness, and in this case there simply is no need to invoke separate lattice structural parameters. A similar approach has been used for several decades in describing the X-ray scattering from superlattice layers in metallic films.[48]

An obvious drawback of model in Figure 2c is that the sharp interfaces in the SLD profile are simply unphysical. The SLD profiles with diffuse interfaces in Figure 2b are more realistic and can be generated by convoluting a Gaussian smoothing function, $g(x)$, with the sharp SLD profile depicted in Figure 2c and eq 4:

$$\rho(x) = \rho'(x) \otimes g(x) \quad (10)$$

$$g(x) = \frac{1}{\sqrt{2\pi}\,\sigma} \exp\left[-\frac{x^2}{2\sigma^2}\right] \quad (11)$$

In eq 11, σ quantifies the width of these diffuse interfaces. Equations 10 and 11 impose the condition that all of the interfaces have identical interfacial widths; this is also a simplification. We also tried a more realistic model with multiple interfacial widths but found that this did not improve the fitting of the SANS data significantly.

All the samples used for the SANS measurements had a thickness of approximately 0.5 mm. For these relatively thick samples the lamellae are randomly distributed in all different orientations relative to the beam, which was evident from the concentric rings in the raw scattering patterns. These conditions warrant the use of the geometric Lorentz correction factor:

$$I(q) = \frac{2\pi I_1(q) G^2(q)}{q^2} \quad (12)$$

to relate eq 9 to the experimentally observed SANS intensity. In this expression, $2\pi/q^2$ is the Lorentz correction factor and $G(q)$ is simply the Fourier transform of the interface gradient function $g(x)$ defined in eq 11 (not shown here).

At this point we have derived an expression to model a lamellar structure with a four layers repeat without resorting to an approximation to decouple the amplitude of the form factor and structure factors. This model works reasonably well to fit all the scattering data as shown by the solid lines in Figure 1. The Gaussian smoothing function in eq 11 not only makes the model more physically meaningful but also improves the fit significantly over a sharp interface mold.

Discussion of the SANS Fitting Results. When fitting eq 12 to the SANS data the following parameters were allowed to vary: the SLD of each layer, the thickness of each layer, and the interfacial width or thickness fluctuation of the layers. The additional constraint was imposed that the volume average of the PPO-rich, PEO-rich, and PAA-rich layers must match the calculated average SLD of the samples based on the known compositions given in Table 1. This was done to ensure the correct overall composition for the sample. The resulting fit parameters and their estimated uncertainties are provided in Table 2. We find that the statistical uncertainty in fitting the model parameters to the experimental scattering data is negligible, typically less than a percent of the fitted values in most cases. A better estimate of the true uncertainty comes

Table 1. Blends of PEO−PPO−PEO Triblock Copolymer and PAA Homopolymer[a]

	mass density[b] (g/cm^3)	SLD[c] (10^{-6} Å^{-2})	electron density (#/Å^3)	vol % in blends: PAA-20[d]	vol % in blends: PAA-30[d]
d-PEO	1.18	6.77	0.355	42.5	37.5
65% d-PPO	1.04	4.42	0.323	38.7	34.1
h-PAA	1.20	1.66	0.381	18.8	28.4
blend SLD[e] (10^{-6} Å^{-2})				4.90	4.52

[a]All data in the table represent values at 70 °C, where the neutron scattering measurements were made. [b]The density data are calculated from *Physical Properties of Polymers Handbook*.[45] [c]The SLD is the sum of the coherent neutron scattering length of the atoms per unit volume. [d]PAA-20 and PAA-30 are for the sample are for blends with PAA loadings of 20% and 30% by mass. [e]The blend's average SLD is the volume average of the three components' SLD, assuming a negligible volume change upon mixing.

DOI: 10.1021/acs.macromol.5b01163
Macromolecules 2015, 48, 7574−7584

Table 2. Model Parameter Derived from the Fitting the SANS Data[a]

20% by mass PAA blend	values fixed by blend composition	values fit from scattering of 88 kg/mol PAA	values fit from scattering of 44 kg/mol PAA	values fit from scattering of 8.5 kg/mol PAA	values fit from scattering of 2 kg/mol PAA
t_{PAA}	0.19	53.0 Å	53.8 Å	52.8 Å	47.6 Å
t_{PEO}(1)	0.21 × 2	14.3 Å	13.7 Å	12.9 Å	12.9 Å
t_{PPO}	0.39	65.0 Å	66.0 Å	67.5 Å	68.0 Å
b_{PAA}(2)	1.66×10^{-6} Å^{-2}	4.86×10^{-6} Å^{-2}	4.85×10^{-6} Å^{-2}	4.85×10^{-6} Å^{-2}	4.85×10^{-6} Å^{-2}
b_{PEO}(2)	6.77×10^{-6} Å^{-2}	5.26×10^{-6} Å^{-2}	5.26×10^{-6} Å^{-2}	5.14×10^{-6} Å^{-2}	5.06×10^{-6} Å^{-2}
b_{PPO}(2)	4.42×10^{-6} Å^{-2}	4.74×10^{-6} Å^{-2}	4.74×10^{-6} Å^{-2}	4.80×10^{-6} Å^{-2}	4.83×10^{-6} Å^{-2}
d_{PAA}	no constraint	7.0 Å	8.2 Å	8.0 Å	8.9 Å
d_{PEO}	no constraint	0 Å	0 Å	0 Å	0 Å
d_{PPO}	no constraint	6.2 Å	7.6 Å	7.5 Å	9.5 Å
D_{total}(3)	no constraint	146.6 Å	147.2 Å	146.1 Å	141.3 Å
b_{total}(4)	4.90×10^{-6} Å^{-2}	4.88×10^{-6} Å^{-2}	4.88×10^{-6} Å^{-2}	4.87×10^{-6} Å^{-2}	4.87×10^{-6} Å^{-2}
30% by mass PAA blend	values fixed by blend composition	values fit from scattering of 88 kg/mol PAA	values fit from scattering of 44 kg/mol PAA	values fit from scattering of 8.5 kg/mol PAA	values fit from scattering of 2 kg/mol PAA
t_A	0.28	78.1 Å	78.5 Å	80.4 Å	75.1 Å
t_E(1)	0.19 × 2	12.8 Å	12.8 Å	11.7 Å	11.6 Å
t_P	0.34	53.3 Å	53.6 Å	53.4 Å	50.6 Å
b_A(2)	1.66×10^{-6} Å^{-2}	4.47×10^{-6} Å^{-2}	4.48×10^{-6} Å^{-2}	4.46×10^{-6} Å^{-2}	4.46×10^{-6} Å^{-2}
b_E(2)	6.77×10^{-6} Å^{-2}	4.65×10^{-6} Å^{-2}	4.75×10^{-6} Å^{-2}	4.65×10^{-6} Å^{-2}	4.62×10^{-6} Å^{-2}
b_P(2)	4.42×10^{-6} Å^{-2}	4.42×10^{-6} Å^{-2}	4.42×10^{-6} Å^{-2}	4.42×10^{-6} Å^{-2}	4.42×10^{-6} Å^{-2}
d_A	no constraint	8.7 Å	6.1 Å	7.7 Å	12.7 Å
d_E	no constraint	0 Å	0 Å	0 Å	0 Å
d_P	no constraint	6.2 Å	5.0 Å	6.8 Å	10.3 Å
D_{total}(3)	no constraint	157.1 Å	157.7 Å	157.1 Å	148.8 Å
b_{total}(4)	4.52×10^{-6} Å^{-2}	4.48×10^{-6} Å^{-2}	4.50×10^{-6} Å^{-2}	4.87×10^{-6} Å^{-2}	4.47×10^{-6} Å^{-2}

[a]A summary of the parameters from fitting the SANS data to the four-layer lamella model described in Figure 2 as a function of the molecular mass of the PAA homopolymer at loadings of 20% (upper panel) and 30% (lower panel) by mass. The variables "t" refer to the thickness, "b" the neutron scattering length density, and "d" the fluctuations in the interfacial width of each layer. The subscripts A, E, and P are used to further denote the PAA, PEO, and PPO layers, respectively. Where appropriate, the second column indicates constraints that were placed on the fitting in terms of the known composition of the blend and the scattering length density of each of the individual components. Note that there are two PEO-rich layers in Figure 2 per repeat unit, and t_E represents the thickness of just one of these layers, such that $D_{total} = t_A + 2t_E + t_P$. As discussed in the main text, the estimated uncertainty in each of the fitted values is on the order of 15%.

from fitting slightly different models to the data. When we compare the fitted values of the parameters between the smeared and sharp interface models to several of the data sets, on average we find the fitted values to vary by 15% across the different parameters. Therefore, we conservatively estimate/report the uncertainty to be 15% of the fitted values.

The total stack thickness, D_{total}, of the repeating unit for the blends with the 2 kg/mol PAA linear homopolymer additives was generally less than those for the higher molecular mass PAA at both the 20% and 30% by mass loadings. D_{total} is approximately 141 Å for the 2k-20 sample versus 146−148 Å for the higher molecular mass PAA at the 20% by mass loading. Likewise, D_{total} is approximately 149 Å for 2k-30 versus 157−158 Å for the higher molecular mass PAA at the 30% by mass loading. These results are consistent with previous SAXS measurements on these same systems.[5,6] With the exception of the low molecular mass sample (2 kg/mol), the three higher molecular mass PAAs (8.5, 44, and 88 kg/mol) show little molecular mass dependence on any of the layer thicknesses, not just the total stack thickness mentioned above. For this reason the rest of this article will focus on the differences between the 2 and 44 kg/mol blends; the 8.5 and 88 kg/mol blends are similar to the 44 kg/mol blends.

The fitted SLD profiles using the Gaussian broadened interface model for the 2 and 44 kg/mol PAA blends are displayed in Figure 3a. These are the SLD profiles used to fit the data presented in Figure 1. However, recall that the average composition within each of the four layers is calculated from the fit data *before* the interface broadening is applied. The sharp interface SLD profile models to determine average composition are presented in Figure 3b−e. This helps simplify the fitting procedure significantly since the composition constraints do not have to be propagated through the convolutions with the interfacial widths. The resulting compositions are summarized in Table 3 for all of the samples studied here. In general, the comparison between the different mass loadings of PAA and the different molecular masses of the PAA additive yield consistent results that seem to make intuitive sense. Here we discuss some of the interesting observations in greater detail.

One of the most striking observations is the consistently diminished values for the interfacial width fluctuation in the PEO rich regions (d_E) in comparison with the d for all the other layers. d_E is essentially zero (fitting consistently yields a value on the order of 0.001) whereas the other layers have thickness fluctuation on the order of 10 Å or so. For this reason all of the d_E values were fixed to zero in all the fits. This is consistent with the notion that a PEO-rich layer results from the localization of PPO−PEO covalent linkage at the interfaces between the PPO-rich and PAA-rich lamellae; i.e., every PEO chain within a PAA-rich lamella is anchored at the above-mentioned interface. The segmental density profile of PEO near the interface is dictated by solution thermodynamics and

DOI: 10.1021/acs.macromol.5b01163
Macromolecules 2015, 48, 7574−7584

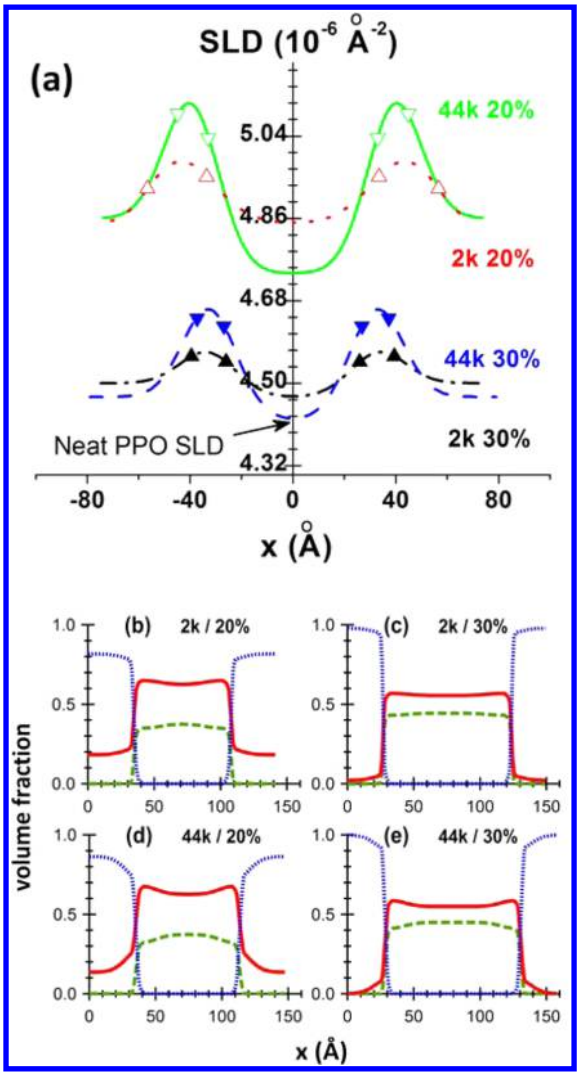

Figure 3. (a) Neutron scattering length density (SLD) profiles of four-layer repeat unit, including the Gausian interfacial broadening, of the PEO−PPO−PEO lamella at loadings of 20% and 30% by mass for both the 2 and 44 kg/mol linear PAA additive. These SLD profiles represent the best fit to SANS data presented in Figure 1. The triangles mark the PEO−PAA and PEO−PPO interface locations before invoking interfacial broadening with the Gaussian function as described in the text. In parts (b) through (e) the fitted SLD profiles are converted into local composition profiles for the PPO (blue dotted lines), PAA (green dashed line), and PEO (red solid line) components for the (b) 2k-20, (c) 2k-30, (d) 44k-20, and (d) 44k-30 blends. These composition profiles were constructed from the SLD profiles prior to symmetric interface broadening using a Gaussian function.

chain connectivity and is not expected to depend significantly on local molecular mass fluctuation. The values of d_P and d_A are generally between 6 and 9 Å, with the largest lamellar width fluctuations occurring in the 2 kg/mol PAA blend; at the highest loading of 30% by mass PAA these value approach 12 Å. That the fluctuations are largest for the lowest molecular mass PAA at high loadings is physically reasonable with the thermodynamics that govern phase separation.

Another interesting feature revealed in Figure 3 and the data presented Tables 2 and 3 is that the extraction of PEO from PPO-rich lamella by the PAA additive is incomplete at 20% mass loading of the PAA, but complete when this is increased to 30% by mass. This is evidenced through the fitted values for

Table 3. Blend Volume Fractions Derived from the SANS Fits[a]

		total volume fractions of component in blend				
blend	component	88k	44k	8.5k	2k	actual
20% PAA	PAA	0.187	0.190	0.187	0.187	0.188
correct	PPO	0.387	0.387	0.387	0.386	0.387
	PEO	0.427	0.424	0.426	0.428	0.425
30% PAA	PAA	0.284	0.283	0.288	0.284	0.284
correct	PPO	0.341	0.341	0.341	0.341	0.341
	PEO	0.375	0.377	0.371	0.375	0.375
20% PAA	PAA	0.219	0.234	0.222	0.286	0.188
incorrect	PPO	0.317	0.291	0.312	0.170	0.387
	PEO	0.464	0.475	0.466	0.544	0.425
30% PAA	PAA	0.193	0.202	0.192	0.232	0.284
incorrect	PPO	0.557	0.528	0.549	0.454	0.341
	PEO	0.250	0.270	0.259	0.314	0.375

[a]Calculated overall compositions of all three components, PAA, PEO, and PPO, for all the materials studied in this work. The sample composition is listed in the last column, and they are the benchmark for the calculated ones to identify a correct composition assignment to a SLD profile. The results in top two rows are calculated under the correct composition assignment whereas the bottom two rows (shaded gray) contain results from incorrect assignments. As discussed in the main text, the estimated uncertainty in each of the fitted values is on the order of 15%.

the SLD of the PPO-rich layer, b_P. The SLD for the neat PPO reported in Table 1 is 4.42×10^{-6}. At the 20% by mass loading of the PAA the SLD of the PPO-rich domain is $(4.7-4.8) \times 10^{-6}$, above the intrinsic SLD of pure PPO which indicates that a fraction of the perdeuterated PEO chains are still present in the lamellae. However, at 30% by mass PAA loading the fitted value of b_P is identical to that of the pure PPO, indicating that no more PEO is present in this layer. This is true for all four of the PAA molecular masses in Tables 2 and 3. Also evident is a concurrent decrease in the PPO layer thickness, t_{PPO}, for the 30% by mass loading PAA over that of 20% by mass loading. That the thickness the PEO plus PPO layer is greater than just the pure PPO layer is also physically reasonable for the formation of a PPO pure layer.

Before discussing these results further, it is important to emphasize some of the implicit assumptions invoked to translate the fitted SLD profiles into compositional profiles. The composition profiles were deduced by assuming that the "PAA-rich" layer is a mixture of just PEO and PAA and that the "PPO-rich" layer is composed of just PPO and PEO. The thin "PEO-rich" layer, which is essentially a transitional layer between the PPO-rich and the PAA -rich lamellae, is assumed to be a mixture of all three components. The PEO-rich lamella has the highest SLD because PEO is the only perdeuterated component in the system and has the highest intrinsic SLD; the PPO and PAA both contain H atoms that lower the SLD as summarized in Table 1.

Both Figure 2 and Table 2 show that there is not a strong difference in SLD between the PPO-rich and PAA-rich layers on either side of the PEO lamella. The strongest scattering contrast is between the PEO-rich lamella and the other layers. This makes the assignment of the PPO-rich layer and the PAA-rich layers somewhat ambiguous. These assignments were done through a trial and error process. After an initial assignment, the resulting compositions of the layers were calculated from the fitted SLDs based on the assumptions of what was in each layer

DOI: 10.1021/acs.macromol.5b01163
Macromolecules 2015, 48, 7574−7584

and a rule of mixtures using the SLD value of the pure components. From the calculated compositions of each layers and their corresponding fitted thicknesses (t_P, t_E, and t_A), the total film composition was calculated. If this composition did not match the known value of the film, the assignment of the PPO- and PAA-rich domains was reversed. All of the fitted profiles presented here are consistent with the known overall composition of the film as summarized in Table 3. The results presented in the first two rows of Table 3 are from the correct composition-SLD assignments for both 20% and 30% by mass PAA loadings. The bottom two rows (shaded gray) are for when the PPO- and PAA-rich layers are reversed. The results from all four PAA molecular masses are included and in the last column the sample compositions are listed. The discrepancy between the experimental values and the calculated ones based on a "wrong" composition assignment is startling. This demonstrates that our assignment of PPO- and PAA-rich layers to certain portions of the SLD profile are well justified. Recall that these composition calculations are based on the SLD profiles prior to interface broadening. Interfacial broadening is not expected to alter the area under SLD profiles and hence not affect the calculations discussed above.

We now return to our discussion of the fitting. At 20% by mass loading of the high molecular mass PAA some PEO remains in the PPO-rich domains. From the SLDs we calculate that the PPO-rich domains are approximately 14% by volume PEO in the 44k-20 sample (Figure 3d). However, when the PAA loading increases to 30% by mass, the PPO phase becomes free of PEO (Figure 3e). These trends are slightly different for the 2 kg/mol PAA additive. The PPO-rich domains of the 2k-20 samples contain about 20% by volume PEO (Figure 3b), significantly more than the 44k-20 sample. With this lowest molecular mass PAA even after the loading increases to 30% by volume, the PPO-rich domains still contain approximately 3% by volume PEO (Figure 3c). We also note that in Figure 1 the SANS peak intensities from samples with the 2 kg/mol PAA are lower than those from samples with higher molecular mass PAA additives. Not surprisingly, the fluctuation amplitude, i.e., the scattering length density contrast, for the 2 kg/mol blends is smaller than those from higher molecular mass PAA samples. One way to think about the role of the PAA additive is a solvent that selectively dissolves the PEO. By selectively solvating the PEO, the PPO gets left behind in a phase-separated domain. However, we observe that the 2 kg/mol PAA is not as good as its higher molecular mass analogues for extracting PEO from PPO. This seems to contradict our general understanding of polymer blends; low molecular mass species are typically better solvents than their high molecular mass counterparts. In this respect it might be better to think about PAA solubility in the PPO. As the PAA molecular mass increases, it becomes increasingly insoluble in the PPO and crashes out of solution while coexisting with the PEO. This appears what drives the physics of self-assembly in this system. Below we will present additional evidence indicating that the PAAs nonsolvent interactions with the PPO are more dominant over the selective solvent interactions with the PEO.

Another important observation that supports this mechanism is that the overall thickness, D_{total}, of the four-layer stack for the 2 kg/mol PAA blends is consistently lower than that of the higher molecular mass blend, as reported in Tables 2. This thinning of the stack thickness is caused by a lateral expansion that increases the lamellar interfacial area as the PAA selectively swells the PEO-rich domains. This is also the reason why D_{total} does not scale with a 0.5 power law with the PAA loadings.[5,6] Given that the extent of thinning in the stack thickness is a reflection of the amount of lateral expansion, the smallest values of D_{total} occur in 2 kg/mol samples is in fact consistent with our understanding of polymer blends; the low molecular mass PAA does seem to do a better job at selectively swelling the PEO domains compared with the higher molecular mass analogues or it is more effective in swelling the PEO layers. This lateral swelling will also decrease the anchoring or the junction density of PEO chains at interfaces; this may contribute to a decrease in the SLD of the PEO rich layers of the 2 kg/mol samples as shown in Figure 3a.

Figure 3a shows an appreciable difference in the neutron SLD profiles between 44k-20 and 44k-30 samples. In contrast, these two samples have very similar electron density profile as given in Figure 4a, deduced from the SLD data given in Table 2

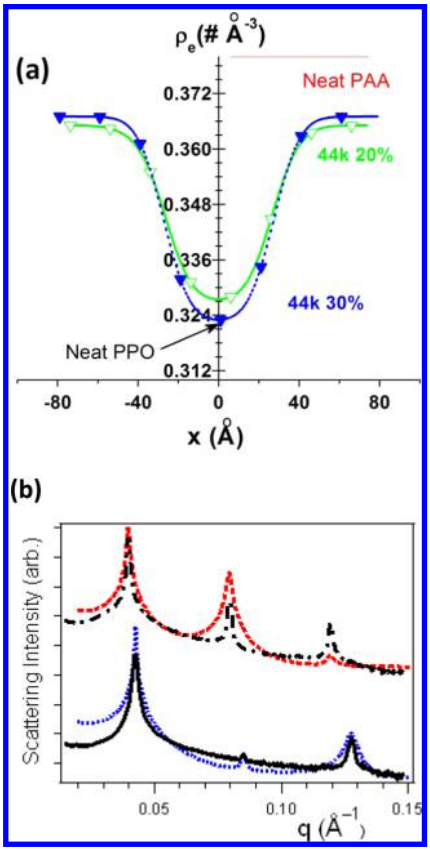

Figure 4. (a) Calculated electron density profile in the blends of PEO−PPO−PEO and PAA of 44 kg/mol at two PAA mass loadings. (B) Experimental SAXS intensities of the 20% PAA 44k (solid line) the 30% PAA 44k (dash-dot line) and the calculated scattering intensity from electron density profiles given above. The q values in the experimental data were rescaled by a factor of 1/1.02; a minor difference in the calibration of the scattering vector between the X-ray and the neutron facilities may exist.

and the intrinsic electron density of the constituent polymers reported in Table 1. A pair of SAXS curves was simulated with the calculated electron density profile and shows excellent agreement with experimental SAXS data provided in Figure 4b. This agreement further verifies our model and fitting results from SANS data. It also demonstrates that SAXS lacks the

DOI: 10.1021/acs.macromol.5b01163
Macromolecules 2015, 48, 7574−7584

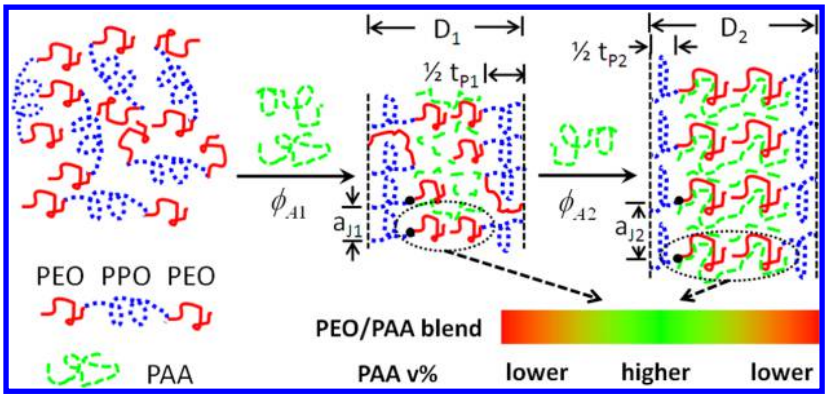

Figure 5. Schematic presentation illustrates the composition distribution within a four-layer stack at two PAA loadings, ϕ_{A1} and ϕ_{A2}. The average distance between PEO−PPO junctions is denoted as a_{j1} and a_{j2} in the above figure. An increase in ϕ_A results in an increase in a_j; this is expected to lower the segmental density of PEO near the BCP junction regions.

contrast to resolve the compositional difference between these two samples.

The SANS results in terms of the distribution of PEO, PPO, and PAA molecules can best be described with the schematic in Figure 5. Before adding PAA, the BCP is in its disordered state shown in the right portion of the figure. Adding 20% by mass (ϕ_{A1}) PAA induces a disorder-to-order transition, and the lamellar structure can be represented as a repeat of many four-layer stacks with a thickness of D_1 given in the middle portion of the figure below and certain portion of PEO remains inside the PPO-rich domains. Adding more PAA to the ordered material results in an increase in both stack thickness D_{total} and distance between BCP junctions denoted as a_j in addition to a pronounced decrease in the thickness of PPO-rich layers. The quantitative results of t_p are given in Table 2, and the increase in a_j is inferred by observing a weak dependence of the stack thickness D_{total} on the PAA loadings.

CONCLUSIONS

In summary, the homopolymer PAA is found to be nearly homogeneously distributed in the PEO blocks for all four molecular weights studied; note that the largest PAA molecule of 88 kg/mol is 20 times that of the PEO blocks, yet it distributes rather uniformly in the PEO blocks. This is in contrast to what been observed in system with a weak homopolymer−BCP interaction. The PAA molecular weight dependence observed in the lamellar structure can be categorized into two groups: low molecular mass PAA of 2 kg/mol and the rest including 8.5k, 44k, and 88k. The 2 kg/mol PAA yields a thinner stack thickness, a lower contrast in its SLD profile, and a larger fluctuation in layer thickness in comparison to the other group. These observations are expected to be useful to guide future theoretical work on the blends between copolymer and homopolymer with strong interspecies interactions, in this case, hydrogen bond formation between PEO block and PAA homopolymer.

METHODS

Equipment and instruments or materials are identified in the paper in order to adequately specify the experimental detail. Such identification does not imply recommendation by NIST, nor does it imply the materials are necessarily the best available for the purpose.

Deuterium-substituted ethylene oxide (98 atomic % D) was purchased from Cambridge Isotope Laboratories, Inc., in a steel cylinder. Deuterated propylene oxide (98 atom % D) was purchased from Sigma-Aldrich. *n*-Butyllithium (1.6 M), propylene glycol (99%), calcium hydride (99%), and potassium (chunks in mineral oil, 98%) were purchased from Sigma-Aldrich and used as received. Propylene oxide was distilled over CaH_2 before the polymerization. Ethylene oxide was condensed in the Schlenk flask at −78 °C and stirred over *n*-BuLi for 1 h at 0 °C and then subsequently condensed to a graduated cylinder connected to reaction Schlenk flask. The 2 kg/mol (high PDI) PAA was purchased from Sigma-Aldrich; 8.5, 44, and 88 kg/mol PAA were purchased from Polymer Source, and these had PDIs of 1.07, 1.08, and 1.12, respectively. Ethanol was purchased from Fisher Scientific.

The PEO−PPO−PEO triblock copolymers are prepared according to a literature procedure by the sequential anionic polymerization of propylene oxide (PO) followed by ethylene oxide (EO).[49] First, initiator made from propylene glycol with freshly cut potassium was added to a weighed dried glass Schlenk flask, which was fitted with a PTFE tap and could be attached to and detached from a vacuum line as needed. Dry PO was transferred into the Schlenk flask by syringe, and the [monomer]/[O^-K^+] ratio was adjusted to control the molecular mass. 65% deuterium substituted propylene oxide was made by mixing 2 mL of deuterium-substituted propylene oxide (98 atomic % D) with 1 mL of hydrogenated propylene oxide. After all the PO was consumed, the required amounts of EO were distilled into the Schlenk flask via the vacuum line through a house manifold assembly.[50] Polymerization was allowed to proceed at 60 °C for 4−6 days. When the polymerization was essentially completed, samples were neutralized by addition of concentrated HCl and evaporation of excess acid and water. The triblock copolymer has a molecular mass of M_n = 12.2 kg/mol and a distribution of PDI = 1.09.

Ethanol solutions of the neat BCP and blends were drop-casted on silicon wafers. Drying was carried out on a hot plate placed inside a vacuum oven with slowly increased vacuum level. The final drying step is 75 °C in a vacuum for 48 h.

SANS measurements were performed at 70 °C on the NG7 30m SANS instrument at the National Institute of Standards and Technology (NIST) in Gaithersburg, MD. Neutrons of wavelength λ = 6 Å with full width at half-maximum $\Delta\lambda/\lambda$ = 11% were used. The data were collected at three sample-to-detector distances (SDD) of 1, 4.5, and 13.5 m. These SDDs cover the high q range from 0.04 1/A to 0.5 1/Å, the mid-q range between 0.007 1/Å and 0.1 1/Å, and the low q range from 0.003 1/Å to 0.032 1/Å. $q = (4\pi/\lambda) \sin\theta$ is the magnitude of the scattering vector, and 2θ is the scattering angle. Scattering intensities were corrected for background scattering, empty cell scattering, and the sensitivity of individual detector pixels. The corrected data sets were placed on an absolute scale using the data reduction software provided by NIST through a direct beam flux method.

SAXS was performed at 80 °C using an instrument from Molecular Metrology Inc. (presently sold as Rigaku S-Max3000) using 1.542 Å (Cu Kα radiation) and an incident beam of 0.4 mm diameter. The sample-to-detector distance was calibrated using silver behenate

DOI: 10.1021/acs.macromol.5b01163
Macromolecules 2015, 48, 7574−7584

standard peak at 0.1076 $Å^{-1}$. The setup employs a two-dimensional gas-filled wire detector for collection of scattered X-ray and allows measurements in wave vector (q) range of $0.006 < q < 0.16$ $Å^{-1}$. The raw scattering data were circularly averaged and plotted as intensity vs q where intensity was used in arbitrary units.

■ ASSOCIATED CONTENT

Supporting Information

The Supporting Information is available free of charge on the ACS Publications website at DOI: 10.1021/acs.macromol.5b01163.

A general formula for the scattering of lamellar stacks with four layers in each repeating stack (PDF)

■ AUTHOR INFORMATION

Corresponding Authors

*E-mail: wen-li.wu@nist.gov (W.L.W.).
*E-mail: csoles@nist.gov (C.L.S.).
*E-mail: watkins@polysci.umass.edu (J.J.W.).

Author Contributions

H.-G.P. and V.K.D. contributed equally to this work.

Notes

The authors declare no competing financial interest.

■ ACKNOWLEDGMENTS

The authors thank Tom Witten and Dan Herbst from the University of Chicago for their thoughtful discussions on interpreting the data.

■ REFERENCES

(1) Mai, Y.; Eisenberg, A. Self-assembly of block copolymers. *Chem. Soc. Rev.* **2012**, *41* (18), 5969−5985.
(2) Warren, S. C.; et al. Ordered Mesoporous Materials from Metal Nanoparticle−Block Copolymer Self-Assembly. *Science* **2008**, *320* (5884), 1748−1752.
(3) Daga, V. K.; et al. Hydrogen Bond Assisted Assembly of Well-Ordered Polyhedral Oligomeric Silsesquioxane-Block Copolymer Composites. *Macromolecules* **2011**, *44* (17), 6793−6799.
(4) Daga, V. K.; et al. Photoinduced Ordering of Block Copolymers. *Nano Lett.* **2011**, *11* (3), 1153−1160.
(5) Daga, V. K.; Watkins, J. J. Hydrogen-Bond-Mediated Phase Behavior of Complexes of Small Molecule Additives with Poly(ethylene oxide-b-propylene oxide-b-ethylene oxide) Triblock Copolymer Surfactants. *Macromolecules* **2010**, *43* (23), 9990−9997.
(6) Tirumala, V. R.; et al. Well-Ordered Polymer Melts with 5 nm Lamellar Domains from Blends of a Disordered Block Copolymer and a Selectively Associating Homopolymer of Low or High Molar Mass. *Macromolecules* **2008**, *41* (21), 7978−7985.
(7) He, J.; et al. On the Influence of Ion Incorporation in Thin Films of Block Copolymers. *Adv. Mater.* **2007**, *19* (24), 4370−4374.
(8) Kim, S. H.; et al. Salt Complexation in Block Copolymer Thin Films. *Macromolecules* **2006**, *39* (24), 8473−8479.
(9) Miranda, D. F.; Russell, T. P.; Watkins, J. J. Ordering in Mixtures of a Triblock Copolymer with a Room Temperature Ionic Liquid. *Macromolecules* **2010**, *43* (24), 10528−10535.
(10) Wang, J.-Y.; et al. Ion Complexation: A Route to Enhanced Block Copolymer Alignment with Electric Fields. *Phys. Rev. Lett.* **2006**, *96* (12), 128301.
(11) Xu, T.; et al. Effect of ionic impurities on the electric field alignment of diblock copolymer thin films. *Colloid Polym. Sci.* **2004**, *282* (8), 927−931.
(12) Lin, Y.; et al. Nanoparticle-Driven Assembly of Block Copolymers: A Simple Route to Ordered Hybrid Materials. *J. Am. Chem. Soc.* **2011**, *133* (17), 6513−6516.
(13) Chiu, J. J.; et al. Control of Nanoparticle Location in Block Copolymers. *J. Am. Chem. Soc.* **2005**, *127* (14), 5036−5037.
(14) Kim, B. J.; et al. Effect of Areal Chain Density on the Location of Polymer-Modified Gold Nanoparticles in a Block Copolymer Template. *Macromolecules* **2006**, *39* (12), 4108−4114.
(15) Jang, S. G.; et al. Synthesis of thermally stable Au-core/Pt-shell nanoparticles and their segregation behavior in diblock copolymer mixtures. *Soft Matter* **2011**, *7* (13), 6255−6263.
(16) Jang, S. G.; Kramer, E. J.; Hawker, C. J. Controlled Supramolecular Assembly of Micelle-Like Gold Nanoparticles in PS-b-P2VP Diblock Copolymers via Hydrogen Bonding. *J. Am. Chem. Soc.* **2011**, *133* (42), 16986−16996.
(17) Wei, Q. S.; et al. Additive-Driven Assembly of Block Copolymer-Nanoparticle Hybrid Materials for Solution Processable Floating Gate Memory. *ACS Nano* **2012**, *6* (2), 1188−1194.
(18) Haryono, A.; Binder, W. H. Controlled Arrangement of Nanoparticle Arrays in Block-Copolymer Domains. *Small* **2006**, *2* (5), 600−611.
(19) Balazs, A. C.; Emrick, T.; Russell, T. P. Nanoparticle Polymer Composites: Where Two Small Worlds Meet. *Science* **2006**, *314* (5802), 1107−1110.
(20) Bockstaller, M. R.; et al. Size-Selective Organization of Enthalpic Compatibilized Nanocrystals in Ternary Block Copolymer/Particle Mixtures. *J. Am. Chem. Soc.* **2003**, *125* (18), 5276−5277.
(21) Bockstaller, M. R.; Mickiewicz, R. A.; Thomas, E. L. Block Copolymer Nanocomposites: Perspectives for Tailored Functional Materials. *Adv. Mater.* **2005**, *17* (11), 1331−1349.
(22) Listak, J.; Bockstaller, M. R. Stabilization of Grain Boundary Morphologies in Lamellar Block Copolymer/Nanoparticle Blends. *Macromolecules* **2006**, *39* (17), 5820−5825.
(23) Thompson, R. B.; et al. Predicting the Mesophases of Copolymer-Nanoparticle Composites. *Science* **2001**, *292* (5526), 2469−2472.
(24) Huh, J.; Ginzburg, V. V.; Balazs, A. C. Thermodynamic Behavior of Particle/Diblock Copolymer Mixtures: Simulation and Theory. *Macromolecules* **2000**, *33* (21), 8085−8096.
(25) Kao, J.; et al. Nanoparticle Assemblies in Thin Films of Supramolecular Nanocomposites. *Nano Lett.* **2012**, *12* (5), 2610−2618.
(26) Kao, J.; et al. Size-Dependent Assemblies of Nanoparticle Mixtures in Thin Films. *J. Am. Chem. Soc.* **2013**, *135* (5), 1680−1683.
(27) Zhao, Y.; et al. Small-molecule-directed nanoparticle assembly towards stimuli-responsive nanocomposites. *Nat. Mater.* **2009**, *8* (12), 979−985.
(28) Thorkelsson, K.; et al. End-to-End Alignment of Nanorods in Thin Films. *Nano Lett.* **2013**, *13* (10), 4908−4913.
(29) Shull, K. R.; Winey, K. I. Homopolymer distributions in lamellar copolymer/homopolymer blends. *Macromolecules* **1992**, *25* (10), 2637−2644.
(30) Winey, K. I.; Thomas, E. L.; Fetters, L. J. Swelling of lamellar diblock copolymer by homopolymer: influences of homopolymer concentration and molecular weight. *Macromolecules* **1991**, *24* (23), 6182−6188.
(31) Winey, K. I.; Thomas, E. L.; Fetters, L. J. Ordered morphologies in binary blends of diblock copolymer and homopolymer and characterization of their intermaterial dividing surfaces. *J. Chem. Phys.* **1991**, *95* (12), 9367−9375.
(32) Tanaka, H.; Hasegawa, H.; Hashimoto, T. Ordered structure in mixtures of a block copolymer and homopolymers. 1. Solubilization of low molecular weight homopolymers. *Macromolecules* **1991**, *24* (1), 240−251.
(33) Hashimoto, T.; Tanaka, H.; Hasegawa, H. Ordered structure in mixtures of a block copolymer and homopolymers. 2. Effects of molecular weights of homopolymers. *Macromolecules* **1990**, *23* (20), 4378−4386.
(34) Hasegawa, H.; et al. SANS and SAXS study of block copolymer/homopolymer mixtures. *J. Appl. Crystallogr.* **1991**, *24* (5), 672−678.
(35) Koizumi, S.; Hasegawa, H.; Hashimoto, T. Spatial Distribution of Homopolymers in Block Copolymer Microdomains As Observed by

DOI: 10.1021/acs.macromol.5b01163
Macromolecules 2015, 48, 7574−7584

a Combined SANS and SAXS Method. *Macromolecules* **1994**, *27* (26), 7893−7906.
(36) Jeon, K.-J.; Roe, R.-J. Solubilization of a Homopolymer in a Block Copolymer. *Macromolecules* **1994**, *27* (9), 2439−2447.
(37) Tirumala, V. R.; et al. Well ordered polymer melts from blends of disordered triblock copolymer surfactants and functional homopolymers. *Adv. Mater.* **2008**, *20* (9), 1603.
(38) Bosse, A. W.; Tirumala, V. R.; Lin, E. K. Tuning block copolymer phase behavior with a selectively associating homopolymer additive. *J. Polym. Sci., Part B: Polym. Phys.* **2009**, *47* (21), 2083−2090.
(39) Dobrosielska, K.; et al. Nanophase-Separated Structures of AB Block Copolymer/C Homopolymer Blends with Complementary Hydrogen-Bonding Interactions. *Macromolecules* **2008**, *41* (20), 7695−7698.
(40) Dobrosielska, K.; et al. Effect of Homopolymer Molecular Weight on Nanophase-Separated Structures of AB Block Copolymer/C Homopolymer Blends with Hydrogen-Bonding Interactions. *Macromolecules* **2009**, *42* (18), 7098−7102.
(41) Tucker, P. S.; Paul, D. R. A simple model for enthalpic effects in homopolymer/block copolymer blends. *Macromolecules* **1988**, *21* (9), 2801−2807.
(42) Quan, X.; et al. Effect of homopolymer molecular weight on the morphology of block copolymer/homopolymer blends. *Macromolecules* **1987**, *20* (6), 1431−1434.
(43) Tirumala, V. R.; et al. Mesoporous silica films with long-range order prepared from strongly segregated block copolymer/homopolymer blend templates. *Chem. Mater.* **2007**, *19* (24), 5868−5874.
(44) Quan, X.; et al. Observation of single-chain scattering from homopolymer blended with a triblock copolymer. *J. Polym. Sci., Part B: Polym. Phys.* **1987**, *25* (3), 641−650.
(45) Mark, J. E. *Physical Property of Polymers*, 3rd ed.; Cambridge University Press: New York, 2004.
(46) Walker, C. B.; Guinier, A. An x-ray investigation of age hardening in alag. *Acta Metall.* **1953**, *1* (5), 568−577.
(47) Guinier, A. *X-Ray Diffraction in Crystals, Imperfect Crystals, and Amorphous Bodies*; W.H. Freeman and Company: San Francisco, 1963.
(48) Fullerton, E. E.; et al. Structural refinement of superlattices from x-ray diffraction. *Phys. Rev. B: Condens. Matter Mater. Phys.* **1992**, *45* (16), 9292−9310.
(49) Altinok, H.; et al. Effect of Block Architecture on the Self-Assembly of Copolymers of Ethylene Oxide and Propylene Oxide in Aqueous Solution. *Langmuir* **1997**, *13* (22), 5837−5848.
(50) Cardoen, G.; et al. Manifold Assembly for the Convenient Polymerization of Ethylene Oxide and Butadiene. *Macromolecules* **2006**, *39* (20), 7170−7173.

DOI: 10.1021/acs.macromol.5b01163
Macromolecules 2015, 48, 7574−7584